JACS
JOURNAL OF THE AMERICAN CHEMICAL SOCIETY

Communication

pubs.acs.org/JACS

Multifunctional Fe_3O_4/TaO_x Core/Shell Nanoparticles for Simultaneous Magnetic Resonance Imaging and X-ray Computed Tomography

Nohyun Lee,[†,∥] Hye Rim Cho,[‡,∥] Myoung Hwan Oh,[†,∥] Soo Hong Lee,[†] Kangmin Kim,[†] Byung Hyo Kim,[†] Kwangsoo Shin,[†] Tae-Young Ahn,[§] Jin Woo Choi,[‡] Young-Woon Kim,[§] Seung Hong Choi,*[,‡] and Taeghwan Hyeon*[,†]

[†]World Class University Program of Chemical Convergence for Energy & Environment, Institute of Chemical Processes, and School of Chemical and Biological Engineering, Seoul National University, Seoul 151-744, Korea

[‡]Diagnostic Radiology, Seoul National University Hospital, and the Institute of Radiation Medicine, Medical Research Center, Seoul National University, 28 Yeongeon-dong, Jongno-gu, Seoul 110-744, Korea

[§]School of Materials Science and Engineering, Seoul National University, Seoul 151-744, Korea

Supporting Information

ABSTRACT: Multimodal imaging is highly desirable for accurate diagnosis because it can provide complementary information from each imaging modality. In this study, a sol–gel reaction of tantalum(V) ethoxide in a microemulsion containing Fe_3O_4 nanoparticles (NPs) was used to synthesize multifunctional Fe_3O_4/TaO_x core/shell NPs, which were biocompatible and exhibited a prolonged circulation time. When the NPs were intravenously injected, the tumor-associated vessel was observed using computed tomography (CT), and magnetic resonance imaging (MRI) revealed the high and low vascular regions of the tumor.

Nanoparticles (NPs) have been intensively studied for their scientific interest and potential applications due to their unique electric, magnetic, and optical properties and their versatile functionality.[1] Biomedical applications of NPs have attracted considerable attention because NPs are expected to improve medical diagnosis and treatment.[2] Properly stabilized NPs smaller than 200 nm have prolonged circulation times, and they accumulate at tumors because of leaky vasculature and poor lymphatic drainage, which is known as the enhanced permeation and retention (EPR) effect.[3] Various NPs have been used as contrast agents for fluorescence imaging, magnetic resonance imaging (MRI), computed tomography (CT), photoacoustic tomography (PAT), and surface-enhanced Raman scattering.[4] Each imaging modality has its own advantages and limitations.[5] For example, CT is advantageous in regard to its high resolution and ease of forming 3D visual reconstruction of tissues of interest, but its inherently low sensitivity results in poor soft-tissue contrast. T_2-weighted MRI using magnetic NPs as contrast agents exhibits high sensitivity and excellent soft-tissue contrast,[6] but intrinsic dark signals of the contrast agents are sometimes confused with other hypointense areas, such as those resulting from air, bleeding, calcification, and metal deposition.[7] Multimodal imaging can overcome these limitations by combining the advantages of each modality.[8] Because NPs can be easily modified or immobilized with biomolecules, fluorescence dyes, and radioisotopes, multifunctional nanoprobes for multimodal imaging can be readily developed [Table S1 in the Supporting Information (SI)].[9] However, most of the previously reported multifunctional nanoprobes have been used for simultaneous imaging of the same region of interest (e.g., tumors); complementary information such as the tumor microenvironment or the development of blood vessels has not been demonstrated to date.[10]

A recently reported TaO_x NP-based CT contrast agent[11] is very promising for clinical applications in comparison with other NP CT contrast agents such as Au and Bi_2S_3 because of its low cost and high biocompatibility.[4c,12] Here we report the synthesis of multifunctional Fe_3O_4/TaO_x core/shell NPs and their use in bimodal CT/MRI. MRI enables discrimination between the oxygenated and hypoxic regions of the tumor, whereas CT shows the tumor-associated blood vessels.

The overall synthesis of the Fe_3O_4/TaO_x core/shell NPs is shown in Scheme 1. Oleic acid-stabilized Fe_3O_4 NPs with average size of 8 nm (Figure 1a) were synthesized by thermal decomposition of an iron–oleate complex using a previously reported procedure with a slight modification.[13] Subsequently, the NPs were incorporated into reverse micelles through mixing with cyclohexane, ethanol, NaOH, and Igepal CO-520. The addition of tantalum(V) ethoxide to the mixture initiated the controlled sol–gel reaction at room temperature, leading to

Scheme 1. Schematic Illustration of Synthesis and Modification of Fe_3O_4/TaO_x Core/Shell NPs

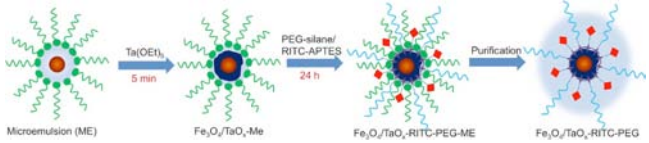

Received: February 20, 2012
Published: June 7, 2012

   dx.doi.org/10.1021/ja3016582 | J. Am. Chem. Soc. 2012, 134, 10309–10312

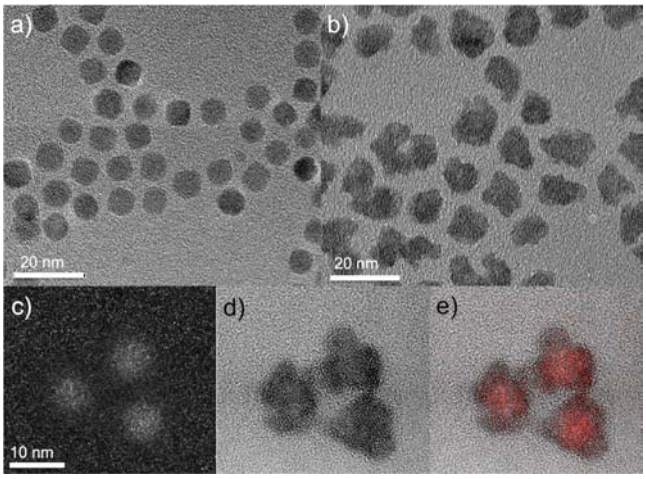

Figure 1. (a, b) TEM images of (a) Fe_3O_4 NPs prepared via thermal decomposition of Fe−oleate complexes and (b) Fe_3O_4/TaO_x core/shell NPs prepared using the Fe_3O_4 NPs. (c) Elemental mapping image for Fe. (d) Bright-field TEM image of Fe_3O_4/TaO_x core/shell NPs. (e) Overlay image of (c) and (d).

the formation of TaO_x shells within 5 min.[11] Finally, the NPs were modified with rhodamine-B isothiocyanate (RITC)-functionalized silane and poly(ethylene glycol) (PEG) silane via a sol−gel reaction between hydroxyl groups on the TaO_x surface and the silane agents, endowing the NPs with fluorescence imaging capability, colloidal stability, and biocompatibility. Figure 1b presents a transmission electron microscopy (TEM) image of the synthesized Fe_3O_4/TaO_x core/shell NPs. Since it was difficult to confirm the core/shell structure with normal TEM images because of the high electron density of Ta, the Fe core was confirmed by electron energy loss spectroscopy (EELS) mapping analysis. In the EELS-mapped image of Fe (Figure 1c), spherical NPs with a size of 8 nm were observed, in very good agreement with the TEM image of the Fe_3O_4 NPs. The superimposed image (Figure 1e) of the elemental mapping image (Figure 1c) on the high-resolution TEM image (Figure 1d) shows that Fe is present mainly in the core region. Because the sol−gel reaction of Ta (V) ethoxide was confined within the microemulsion, core/shell structures were successfully generated. The incorporation of Fe_3O_4 NPs into reverse micelles did not seem to affect the structure of the microemulsion, and the size and shape of the resulting NPs were similar up to an Fe_3O_4 NP concentration of 0.4 mg/mL (Figure S1 in the SI). Some free TaO_x NPs that did not contain Fe_3O_4 were also obtained at low Fe_3O_4 NP concentrations (Figure S2). Because of the high sensitivity of MRI relative to CT, Fe_3O_4/TaO_x core/shell NPs synthesized at an Fe_3O_4 NP concentration of 0.2 mg/mL were used for the subsequent studies.

The Fe_3O_4/TaO_x core/shell NPs exhibited excellent colloidal stability in aqueous media due to their stabilization by PEG. The hydrodynamic diameter of the NPs measured using dynamic light scattering (DLS) was ∼21 nm in water (Figure S3a), and no aggregation was observed over 1 month. The field-dependent magnetization curve of the Fe_3O_4/TaO_x core/shell NPs showed that the NPs were superparamagnetic at room temperature, which is an important characteristic for T_2 contrast agents (Figure S3b). The NPs exhibited the emission peak of rhodamine B at 580 nm, demonstrating their potential for fluorescence imaging (Figure S3c).

X-ray CT and MRI images of a phantom were obtained at various concentrations of Fe_3O_4/TaO_x core/shell NPs dispersed in deionized water. In the CT images, the signal increased linearly with the NP concentration (Figure 2a,b). T_2-

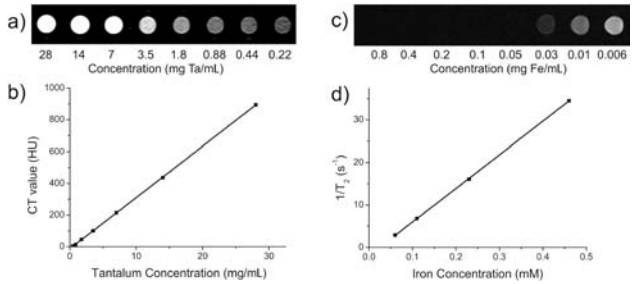

Figure 2. (a) CT phantom images at various concentrations of Fe_3O_4/TaO_x core/shell NPs and (b) HU values. (c) T_2-weighted MRI image of the same phantom and (d) R_2 values.

weighted MRI images of the same phantom were acquired using a 3 T MRI scanner. As the NP concentration increased, the signal intensity decreased significantly (Figure 2c). The measured r_2 value was 81.156 mM^{-1} s^{-1} (Figure 2d). Whereas the signal intensity of the CT image continuously increased without saturation, the T_2 contrast effect of the NPs saturated at a concentration of 0.05 mg Fe/mL, and further signal attenuation was not observed above this concentration. However, a sufficient T_2 contrast effect was observed at low concentration because of the high sensitivity of MRI.

The cytotoxicity of Fe_3O_4/TaO_x NPs was evaluated with a 3-(4,5-dimethylthiazol-2-yl)-2,5-diphenyltetrazolium bromide (MTT) assay using a murine macrophage cell line (RAW 264.7). The macrophage cell line was chosen because most administered foreign materials are cleared by professional phagocytes of the monocyte/macrophage lineage.[14] No appreciable toxicity was observed up to a concentration of 4.3 mg/mL (Figure S4a). This high biocompatibility is a great advantage of Fe_3O_4/TaO_x NPs. Although FePt NPs[15] and Gd-chelate-coated gold NPs[12c] were used for bimodal CT/MRI, these NPs have inherent limitations in clinical applications because leached Pt or Gd ions are known to be toxic.[16,17] In contrast, Fe_3O_4 and TaO_x are biocompatible materials that have been clinically used as MRI contrast agents and stents, respectively.[18]

Cellular uptake was investigated after incubation of RAW 264.7 cells with Fe_3O_4/TaO_x core/shell NPs for 24 h. The internalized NPs were observed in the cytoplasm as red fluorescence (Figure S4b). After the cellular uptake was confirmed, in vitro CT and MRI images of the cells incubated with various concentrations of NPs were obtained. As the concentration increased, the signals of the cells increased and decreased in the CT and MRI images, respectively (Figure S4c,d).

To assess the feasibility of in vivo bimodal CT/MR imaging of the tumor, rats were subcutaneously inoculated with rat mammary adenocarcinoma cells (MAT B III). The tumors were allowed to grow to a size of ∼1 cm in diameter, resulting in an inhomogeneous interior. Subsequently, Fe_3O_4/TaO_x core/shell NPs (840 mg/kg) were injected intravenously into the tail veins of the rats. Such a high dose of the NPs was chosen because of the low sensitivity of CT. Dual MR/CT imaging was performed using a clinical CT and MRI scanner before and after tail-vein injection of the NPs. After

dx.doi.org/10.1021/ja3016582 | J. Am. Chem. Soc. 2012, 134, 10309−10312

administration of the NPs, preferential signal enhancement of blood vessels, including the tumor-associated vessel, was observed in volume-rendered CT images (Figure 3 and Figures

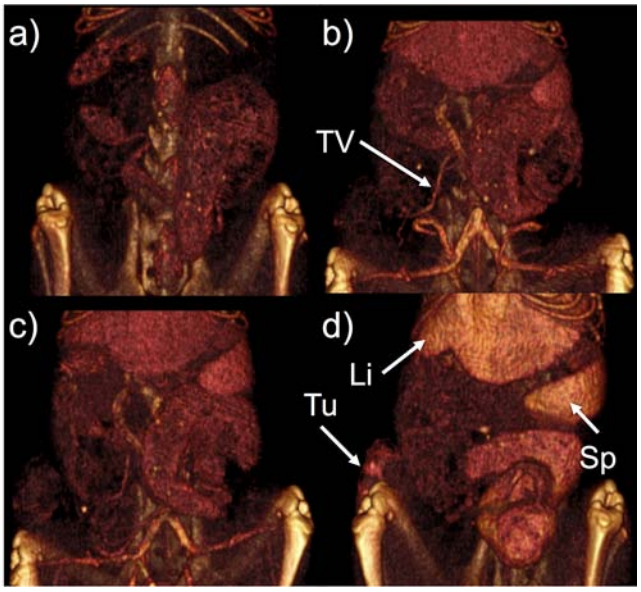

Figure 3. In vivo X-ray CT images of a rat (a) before and (b) 1 h, (c) 2 h, and (d) 24 h after the injection of Fe_3O_4/TaO_x core/shell NPs (840 mg/kg). TV, Li, Tu, and Sp indicate the tumor-associated vessel, liver, tumor, and spleen, respectively.

S5 and S6). While clinically available iopromide solution (Ultravist 370, 740 mg I/kg) caused a slight signal enhancement for a few minutes (Figure S7), the signal of the NPs in blood vessels was stronger and persisted for more than 2 h. 3D imaging of the blood vessels using CT is advantageous for tumor therapy because the tumor-associated vessel is one of the main targets in effective cancer treatment.[19] Despite the high sensitivity of T_2-weighted MRI, blood-pool imaging is known to be difficult because T_2 contrast agents reduce the signal of the region of interest. The NPs accumulated at the tumor via the EPR effect and were cleared by the reticuloendothelial system (RES). Consequently, the Hounsfield unit (HU) values for the blood vessels decreased slowly, while those for the tumor, liver, and spleen gradually increased (Table S2). However, in contrast with the liver and spleen, the exact shape and structure of the tumor were not revealed because of the low sensitivity of CT and the inhomogeneous distribution of the NPs.

On the other hand, T_2-weighted MRI was able to capture the detailed structure of the tumor. Before intravenous injection of the NPs, the tumor appeared homogeneous and bright in the MRI image (Figure 4a). After administration of the NPs, the tumor appeared inhomogeneous, though the overall signal of the tumor was significantly attenuated (Figure 4). The signal reduction in the peripheral region of the tumor was so severe that this region appeared very dark, whereas the tumor core became gray. Histological observation of the dissected tumor slice revealed that the inhomogeneous tumor consisted of a peripheral oxygenated region and a hypoxic core region (Figure S8).[20] The cells in the peripheral region seemed to be healthy because sufficient oxygen and nutrients were supplied by peripheral vasculatures. When the tumor slices were observed using fluorescence microscopy, the NPs were found mainly in these peripheral regions around the blood vessels (Figure S9).

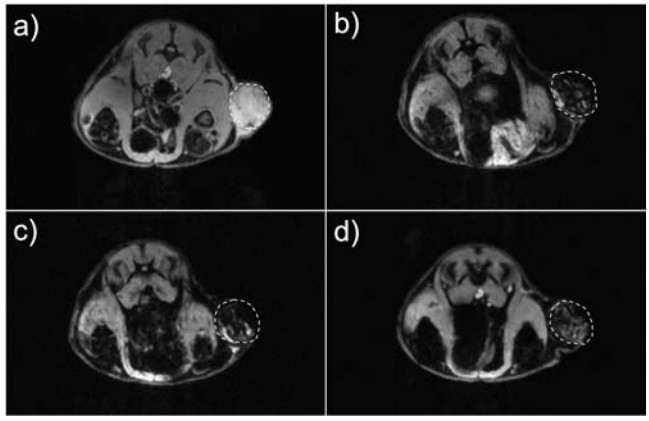

Figure 4. In vivo T_2-weighted MRI images of a rat bearing a MAT III B tumor (a) before and (b) 1 h, (c) 2 h, and (d) 24 h after the injection of Fe_3O_4/TaO_x core/shell NPs (840 mg/kg).

Because of the limited vasculature, delivery of antitumor agents to a hypoxic tumor core is known to be very difficult.[21] This is problematic, since the surviving cells in the inaccessible hypoxic region can be the source of tumor recurrence after therapy.[22] Because the hypoxic and oxygenated regions can be distinguished using MRI, the Fe_3O_4/TaO_x core/shell NPs can help to determine an effective method of tumor treatment.

Fluorescence images of the sections of the major organs, including the liver, spleen, kidney, and heart, showed that the NPs were mainly cleared by the liver and spleen (Figure S10). The fluorescence of the NPs was observed 14 days after administration, indicating that degradation of the NPs is very slow or unlikely to occur. To show the biocompatibility of Fe_3O_4/TaO_x NPs, the toxicity of the NPs in rats was intensively studied. Most of the serum chemistry and hematological parameters were normal for 14 days after intravenous injection of the NPs (Figure S11 and Table S3). Although several parameters, including aspartate aminotransferase (AST) and alanine aminotransferase (ALT), were slightly elevated, they returned to normal within a week. In addition, no apparent change in the histology of the major organs was observed (Figure S12). Fe_3O_4/TaO_x core/shell NPs synthesized with an increased amount of Fe_3O_4 NPs failed to produce appropriate MR images because the signals from most of the internal organs were severely reduced (Figure S13).

In conclusion, bimodal CT/MRI was successfully demonstrated using biocompatible Fe_3O_4/TaO_x core/shell NPs. The multifunctional core/shell NPs can provide complementary information from CT and MRI. Newly formed blood vessels to the tumors can be clearly imaged by CT, and the tumor microenvironment, including the hypoxic and oxygenated regions, can be evaluated using MRI. These core/shell NPs have enormous potential for accurate cancer diagnosis through visualization of developed tumor vessels, monitoring of tumor status, and anticipation of therapy.

■ ASSOCIATED CONTENT

Ⓢ Supporting Information

Detailed experimental procedures, TEM images of Fe_3O_4/TaO_x core/shell NPs, DLS data, $M-H$ curve, fluorescence spectrum, MTT data, fluorescence image of labeled cells, in vitro CT and MRI images, whole-body CT image of a rat, hematoxylin/eosin-stained sections of organs, and fluorescence image of the

dx.doi.org/10.1021/ja3016582 | J. Am. Chem. Soc. 2012, 134, 10309−10312

tumor section. This material is available free of charge via the Internet at http://pubs.acs.org.

AUTHOR INFORMATION

Corresponding Author

choiseunghong@gmail.com; thyeon@snu.ac.kr

Author Contributions

[‖]N.L., H.R.C., and M.H.O. contributed equally.

Notes

The authors declare no competing financial interest.

ACKNOWLEDGMENTS

T.H. acknowledges financial support by the National Research Foundation (NRF) of Korea through the Strategic Research (2010-0029138), Global Research Laboratory (2011-0021628), and World Class University (R31-10013) Programs. S.H.C. acknowledges financial support from the Korea Healthcare Technology R&D Projects, Ministry for Health, Welfare & Family Affairs (A112028).

REFERENCES

(1) (a) *Nanoscale Materials in Chemistry*; Klabunde, K. J., Ed.; Wiley-Interscience: New York, 2001. (b) Ozin, G. A.; Arsenault, A.; Cademartiri, L. *Nanochemistry: A Chemical Approach to Nanomaterials*, 2nd ed.; RSC Publishing: Cambridge, U.K., 2008. (c) Schmid, G. *Nanoparticles: From Theory to Application*; Wiley-VCH: Weinheim, Germany, 2004. (d) Somorjai, G. A.; Frei, H.; Park, J. Y. *J. Am. Chem. Soc.* **2009**, *131*, 16589.

(2) (a) *Nanobiotechnology: Concepts, Applications and Perspectives*; Niemeyer, C. M., Mirkin, C. A., Eds.; Wiley-VCH: Weinheim, Germany, 2004. (b) Ho, D.; Sun, X.; Sun, S. *Acc. Chem. Res.* **2011**, *44*, 875. (c) Yoo, D.; Lee, J.-H.; Shin, T.-H.; Cheon, J. *Acc. Chem. Res.* **2011**, *44*, 863. (d) Bhirde, A.; Xie, J.; Swierczewska, M.; Chen, X. *Nanoscale* **2011**, *3*, 142. (e) Gao, J.; Xu, B. *Nano Today* **2009**, *4*, 37.

(3) (a) Gao, X.; Cui, Y.; Levenson, R. M.; Chung, L. W. K.; Nie, S. *Nat. Biotechnol.* **2004**, *22*, 969. (b) Perrault, S. D.; Walkey, C.; Jennings, T.; Fischer, H. C.; Chan, W. C. W. *Nano Lett.* **2009**, *9*, 1909.

(4) (a) Choi, H. S.; Liu, W.; Liu, F.; Nasr, K.; Misra, P.; Bawendi, M. G.; Frangioni, J. V. *Nat. Nanotechnol.* **2009**, *5*, 42. (b) Jun, Y.-w.; Lee, J.-H.; Cheon, J. *Angew. Chem., Int. Ed.* **2008**, *47*, 5122. (c) Rabin, O.; Perez, J. M.; Grimm, J.; Wojtkiewicz, G.; Weissleder, R. *Nat. Mater.* **2006**, *5*, 118. (d) Kim, C.; Favazza, C.; Wang, L. V. *Chem. Rev.* **2010**, *110*, 2756. (e) Qian, X.; Peng, X.-H.; Ansari, D. O.; Yin-Goen, Q.; Chen, G. Z.; Shin, D. M.; Yang, L.; Young, A. N.; Wang, M. D.; Nie, S. *Nat. Biotechnol.* **2008**, *26*, 83.

(5) Willmann, J. K.; van Bruggen, N.; Dinkelborg, L. M.; Gambhir, S. S. *Nat. Rev. Drug Discovery* **2008**, *7*, 591.

(6) Lee, N.; Kim, H.; Choi, S. H.; Park, M.; Kim, D.; Kim, H.-C.; Choi, Y.; Lin, S.; Kim, B. H.; Jung, H. S.; Kim, H.; Park, K. S.; Moon, W. K.; Hyeon, T. *Proc. Natl. Acad. Sci. U.S.A.* **2011**, *108*, 2662.

(7) Na, H. B.; Song, I. C.; Hyeon, T. *Adv. Mater.* **2009**, *21*, 2133.

(8) (a) Gao, J.; Gu, H.; Xu, B. *Acc. Chem. Res.* **2009**, *42*, 1097. (b) Kim, J.; Piao, Y.; Hyeon, T. *Chem. Soc. Rev.* **2009**, *38*, 372. (c) Lee, D.-E.; Koo, H.; Sun, I.-C.; Ryu, J. H.; Kim, K.; Kwon, I. C. *Chem. Soc. Rev.* **2012**, *41*, 2656.

(9) (a) Lee, J. E.; Lee, N.; Kim, T.; Kim, J.; Hyeon, T. *Acc. Chem. Res.* **2011**, *44*, 893. (b) Selvan, S. T.; Patra, P. K.; Ang, C. Y.; Ying, J. Y. *Angew. Chem., Int. Ed.* **2007**, *46*, 2448. (c) So, M.-K.; Xu, C.; Loening, A. M.; Gambhir, S. S.; Rao, J. *Nat. Biotechnol.* **2006**, *24*, 339. (d) Choi, J.-s.; Park, J. C.; Nah, H.; Woo, S.; Oh, J.; Kim, K. M.; Cheon, G. J.; Chang, Y.; Yoo, J.; Cheon, J. *Angew. Chem., Int. Ed.* **2008**, *47*, 6259. (e) Kim, D.; Yu, M. K.; Lee, T. S.; Park, J. J.; Jeong, Y. Y.; Jon, S. *Nanotechnology* **2011**, *22*, 155101.

(10) (a) Moore, A.; Medarova, Z.; Potthast, A.; Dai, G. *Cancer Res.* **2004**, *64*, 1821. (b) Kievit, F. M.; Stephen, Z. R.; Veiseh, O.; Arami, H.; Wang, T.; Lai, V. P.; Park, J. O.; Ellenbogen, R. G.; Disis, M. L.; Zhang, M. *ACS Nano* **2012**, *6*, 2591. (c) Lee, H.; Yu, M. K.; Park, S.; Moon, S.; Min, J. J.; Jeong, Y. Y.; Kang, H.-W.; Jon, S. *J. Am. Chem. Soc.* **2007**, *129*, 12739.

(11) (a) Oh, M. H.; Lee, N.; Kim, H.; Park, S. P.; Piao, Y.; Lee, J.; Jun, S. W.; Moon, W. K.; Choi, S. H.; Hyeon, T. *J. Am. Chem. Soc.* **2011**, *133*, 5508. (b) Bonitatibus, P. J., Jr.; Torres, A. S.; Goddard, G. D.; FitzGerald, P. F.; Kulkarni, A. M. *Chem. Commun.* **2010**, *46*, 8956.

(12) (a) Kim, D.; Park, S.; Lee, J. H.; Jeong, Y. Y.; Jon, S. *J. Am. Chem. Soc.* **2007**, *129*, 7661. (b) Kinsella, J. M.; Jimenez, R. E.; Karmali, P. P.; Rush, A. M.; Kotamraju, V. R.; Gianneschi, N. C.; Ruoslahti, E.; Stupack, D.; Sailor, M. J. *Angew. Chem., Int. Ed.* **2011**, *50*, 12308. (c) Alric, C.; Taleb, J.; Le Duc, G.; Mandon, C.; Billotey, C.; Le Meur-Herland, A.; Brochard, T.; Vocanson, F.; Janier, M.; Perriat, P.; Roux, S.; Tillement, O. *J. Am. Chem. Soc.* **2008**, *130*, 5908. (d) Popovtzer, R.; Agrawal, A.; Kotov, N. A.; Popovtzer, A.; Balter, J.; Carey, T. E.; Kopelman, R. *Nano Lett.* **2008**, *8*, 4593. (e) Sun, I.-C.; Eun, D.-K.; Koo, H.; Ko, C.-Y.; Kim, H.-S.; Yi, D. K.; Choi, K.; Kwon, I. C.; Kim, K.; Ahn, C.-H. *Angew. Chem., Int. Ed.* **2011**, *50*, 9348.

(13) Park, J.; An, K.; Hwang, Y.; Park, J.-G.; Noh, H.-J.; Kim, J.-Y.; Park, J.-H.; Hwang, N.-M.; Hyeon, T. *Nat. Mater.* **2004**, *3*, 891.

(14) Pan, Y.; Neuss, S.; Leifert, A.; Fischler, M.; Wen, F.; Simon, U.; Schmid, G.; Brandau, W.; Jahnen-Dechent, W. *Small* **2007**, *3*, 1941.

(15) Chou, S.-W.; Shau, Y.-H.; Wu, P.-C.; Yang, Y.-S.; Shieh, D.-B.; Chen, C.-C. *J. Am. Chem. Soc.* **2010**, *132*, 13270.

(16) (a) Gao, J.; Liang, G.; Zhang, B.; Kuang, Y.; Zhang, X.; Xu, B. *J. Am. Chem. Soc.* **2007**, *129*, 1428. (b) Asharani, P.; Xinyi, N.; Hande, M. P.; Valiyaveettil, S. *Nanomedicine* **2010**, *5*, 51.

(17) (a) Sieber, M. A.; Steger-Hartmann, T.; Lengsfeld, P.; Pietsch, H. *J. Magn. Reson. Imaging* **2009**, *30*, 1268. (b) Perazella, M. A. *Clin. J. Am. Soc. Nephrol.* **2009**, *4*, 461.

(18) (a) Harisinghani, M. G.; Barentsz, J.; Hahn, P. F.; Deserno, W. M.; Tabatabaei, S.; van de Kaa, C. H.; de la Rosette, J.; Weissleder, R. *N. Engl. J. Med.* **2003**, *348*, 2491. (b) Chen, J. Y.; Leng, Y. X.; Tian, X. B.; Wang, L. P.; Huang, N.; Chu, P. K.; Yang, P. *Biomaterials* **2002**, *23*, 2545.

(19) McDonald, D. M.; Choyke, P. L. *Nat. Med.* **2003**, *9*, 713.

(20) Harris, A. L. *Nat. Rev. Cancer* **2002**, *2*, 38.

(21) Primeau, A. J.; Rendon, A.; Hedley, D.; Lilge, L.; Tannock, I. F. *Clin. Cancer Res.* **2005**, *11*, 8782.

(22) Lewis, C.; Murdoch, C. *Am. J. Pathol.* **2005**, *167*, 627.